PAPER

MST resistive wall tearing mode simulations

IOP Publishing Plasma Physics and Controlled Fusion
Plasma Phys. Control. Fusion **65** (2023) 084002 (7pp) https://doi.org/10.1088/1361-6587/acdff8

MST resistive wall tearing mode simulations

H R Strauss[1,*], B E Chapman[2] and N C Hurst[2]

[1] HRS Fusion, West Orange, NJ 07052, United States of America
[2] Dept. of Physics, University of Wisconsin-Madison, Madison, WI 53706, United States of America

E-mail: hank@hrsfusion.com

Received 23 February 2023, revised 28 April 2023
Accepted for publication 20 June 2023
Published 29 June 2023

Abstract

The Madison Symmetric Torus (MST) is a toroidal device that, when operated as a standard tokamak, does not have major disruptions. Unlike most tokamaks, the MST plasma is surrounded by a close fitting highly conducting wall, with a resistive wall penetration time two orders of magnitude longer than in JET or DIII-D, and three times longer than in ITER. The MST can operate with edge $q_a \leqslant 2$, unlike standard tokamaks. Simulations presented here indicate that the MST is unstable to resistive wall tearing modes (RWTMs) and resistive wall modes (RWMs). They could in principle cause disruptions, but the predicted thermal quench (TQ) time is much longer than the experimental pulse time. If the MST TQ time were comparable to measurements in JET and DIII-D, theory and simulations predict that disruptions would have been observed in MST. This is consistent with the modeling herein, predicting that disruptions are caused by RWTMs and RWMs. In the low $q_a \sim 2$ regime of MST, the RWTM asymptotically satisfies the RWM dispersion relation. The transition from RWTM to RWM occurs smoothly at $q_a = m/n$, where m, n are poloidal and toroidal mode numbers.

Keywords: tokamak, disruption, MST, RWTM, thermal quench

(Some figures may appear in colour only in the online journal)

1. Introduction

Tokamaks are subject to disruptions, events in which thermal and magnetic energy confinement is lost. It was not known what instability causes the thermal quench (TQ) in disruptions. Disruptions have been predicted to be a severe problem in large future devices such as ITER. Previous studies of JET [1], ITER [2], DIII-D [3] showed that disruptions can be caused by resistive wall tearing modes (RWTMs). These are tearing modes (TMs) whose resonant surface is inside the plasma, but is close to the wall. With a perfectly conducting wall, the TMs are stable, but with no wall, they are unstable. The TQ time is proportional to the RWTM growth time. With a highly conducting wall, the growth time is of order the resistive wall penetration time. In the Madison Symmetric Torus (MST) [4, 5] the growth time is much longer than the shot duration.

The main result of this paper is that the predicted TQ time in MST is much longer than in conventional tokamaks such as JET and DIII-D, and is longer than a prediction for ITER based on RWTMs. This is shown in figure 1. The TQ time in ms is shown as a function of $S_{\rm wall}$, the resistive wall penetration time normalized to the Alfvén time (defined below). For JET and DIII-D, the TQ time is based on experimental data and simulations. For ITER and MST, the TQ time is based on simulation. The MST case is for $q_a = 2.6$, described in more detail below. In MST, a TQ does not occur during the experimental shot duration, which gives a lower limit to the possible TQ time. This paper does not propose that a long $\tau_{\rm wall}$ will eliminate disruptions, but that it can mitigate them. The TQ time is extended so the disruption thermal load will be much more tolerable than with more resistive walls.

Another result is that in the low edge safety factor $q_a \leqslant 2.6$ regime of MST, the RWTM growth time scales linearly in the resistive wall penetration time [3]. This is characteristic of large $S_{\rm wall}$, in which the RWTM asymptotically satisfies

* Author to whom any correspondence should be addressed.

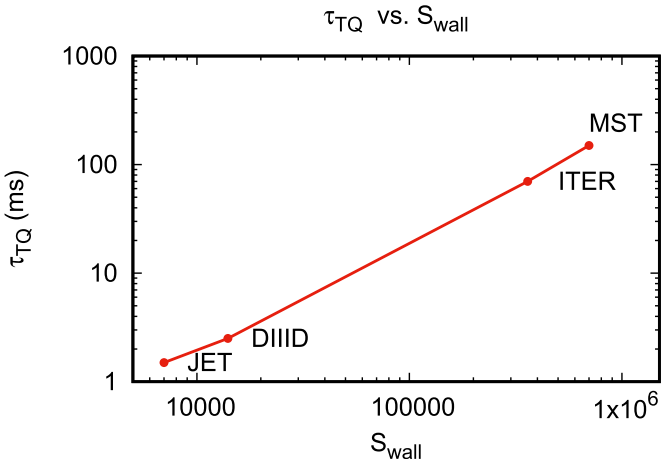

Figure 1. TQ time in ms as a function of $S_{\rm wall}$—measured (JET, DIII-D) and simulated (ITER, MST).

the resistive wall mode (RWM) dispersion relation. ITER could also be in this regime. The largest amplitude magnetic perturbation seen in simulations is the RWTM with rational surface radius $r_{\rm s}$ at which $q(r_{\rm s}) = m/n$ is closest to q_a, although RWMs can have a comparable amplitude.

The MST experiment is a toroidal device which can be operated as a reversed field pinch (RFP) or as a tokamak. It is well known [6] that RFPs require a highly conducting wall, or feedback, in order to stabilize external kink modes. The MST device is shown in figure 2. It has a circular cross section with limiters, a single-turn TF winding, PF windings wrapped around an iron-core transformer, and a close-fitting conducting shell with wall penetration time $\tau_{\rm wall} = 800\,$ms.

The MST wall penetration time is more than three times longer than in ITER, with [7] $\tau_{\rm wall} = 250\,$ms. MST has a pulse time of about 50 ms, during which the wall is effectively an ideal conductor. It can operate with $q_a \leqslant 2$ [5]. No disruptions have been seen to date when it is operated as a standard tokamak. Disruptions can occur under non standard conditions with very low density, in discharges dominated by runaway electrons. It has internal MHD modes, including $(1,1)$ internal kinks, which produce sawteeth. According to the theory and simulations presented here, disruptions are suppressed by the highly conducting wall. Similar low q_a stability has been obtained by use of feedback stabilization [8].

In the following, theory and simulations are presented which indicate that MST is unstable to RWTMs and RWMs, which could cause disruptions in conventional tokamaks [1–3]. These results suggest that disruptions are not observed in MST because the predicted TQ time $\tau_{\rm TQ}$ is much longer than the experimental pulse duration. It is shown that RWTMs and RWMs in MST have the same mode growth time scaling linearly in the resistive wall magnetic penetration time $\tau_{\rm wall}$. It is also shown that there is a smooth transition from RWTMs to RWMs when the rational surface exits the plasma.

Simulations were done to obtain the scaling of the TQ time $\tau_{\rm TQ}$ with wall resistivity. The simulations were performed with the nonlinear resistive MHD M3D code [9] with a resistive wall [10]. Simulations were initialized with MSTFit [11] equilibria having on axis $q_0 = 1$, and several values of edge $q = q_a$ in the range $1.5 \leqslant q_a \leqslant 2.6$. The parameters were: Lundquist number $S = 10^5$ (the experimental value), and parallel thermal conductivity $\chi_\parallel = 10R^2/\tau_{\rm A}$, (somewhat larger than the experimental value $4R^2/\tau_{\rm A}$). The experiment has $B_T = 0.133\,$T, and average density $n_e = 4.5 \times 10^{12}\,{\rm cm}^{-3}$. The major radius is $R = 1.5\,$m, and the minor radius is 0.52 m. The fill gas was deuterium. The volume averaged $\beta \approx 5 \times 10^{-3}$, and the Alfvén time is $\tau_{\rm A} = R/v_{\rm A} = 1.15 \times 10^{-6}\,$s. The resistive wall time is $\tau_{\rm wall} = \mu_0 \delta_{\rm w} r_{\rm w}/\eta_{\rm w}$, where $\delta_{\rm w}$ is the wall thickness, $r_{\rm w}$ is the wall radius, and $\eta_{\rm w}$ is the wall resistivity. With $\tau_{\rm wall} = .8\,$s, then $S_{\rm wall} = \tau_{\rm wall}/\tau_{\rm A} = 7 \times 10^5$. The value of $S = 10^5$, which gives $T = 69\,$eV on axis. The resistivity varied as $T^{-3/2}$, with a cutoff at 1% of the initial maximum T. The density was taken as constant, and the pressure was proportional to T. The parallel conductivity in the collisional regime is $\chi_\parallel = 2.1 v_{te}^2 \tau_e$, or $\chi_\parallel = 8 \times 10^{11}\,{\rm cm}^2\,{\rm s}^{-1}$. This can be expressed as $\chi_\parallel = 4.1R^2/\tau_{\rm A}$. The simulations do not include rotation, which has a stabilizing effect [12–14] on RWTMs. The computational plasma extended to the wall, and the narrow limiters were not explicitly taken into account.

2. RWTM theory

This section reviews some theory of RWTMs and RWMs. The RWTM dispersion relation [1, 15] is

$$S^{3/4} S_{\rm wall}^{-5/4} (\hat\gamma^{9/4} + g_{\rm s} \hat\gamma^{5/4}) = \Delta_i \hat\gamma + g_{\rm s} \Delta_n \qquad (1)$$

where $\hat\gamma = \gamma \tau_{\rm wall}$, S is the Lundquist number, $g_{\rm s} = 2m/[1 - (r_{\rm s}/r_{\rm w})^{2m}]$, ideal wall stability parameter $\Delta_i = r_{\rm s} \Delta'_{\rm ideal}/m$, external stability parameter $\Delta_x = 2r_{\rm s}^{2m}/(r_{\rm w}^{2m} - r_{\rm s}^{2m})$, with rational surface radius $r_{\rm s}$, in a cylindrical geometry large aspect ratio model. The no wall stability parameter is $\Delta_n = \Delta_i + \Delta_x$. RWTMs have $\Delta_i \leqslant 0$, and require finite $S_{\rm wall}$. The RWTM growth rate scalings vary as $\gamma \propto S^{-\alpha}$, with $4/9 \leqslant \alpha \leqslant 1$. In a JET example [1], $\alpha = 4/9$, while in a DIII-D example [3] $\alpha = 2/3$.

In the following MST examples, $\gamma \sim \tau_{\rm wall}^{-1}$, $\alpha = 1$. This is because of the smallness of the coefficient on the left side of (1). With MST parameters, $S^{3/4} S_{\rm wall}^{-5/4} = 2.8 \times 10^{-4}$. The left side of (1) is only significant when Δ_i is within a small range of $\Delta_i = 0$.

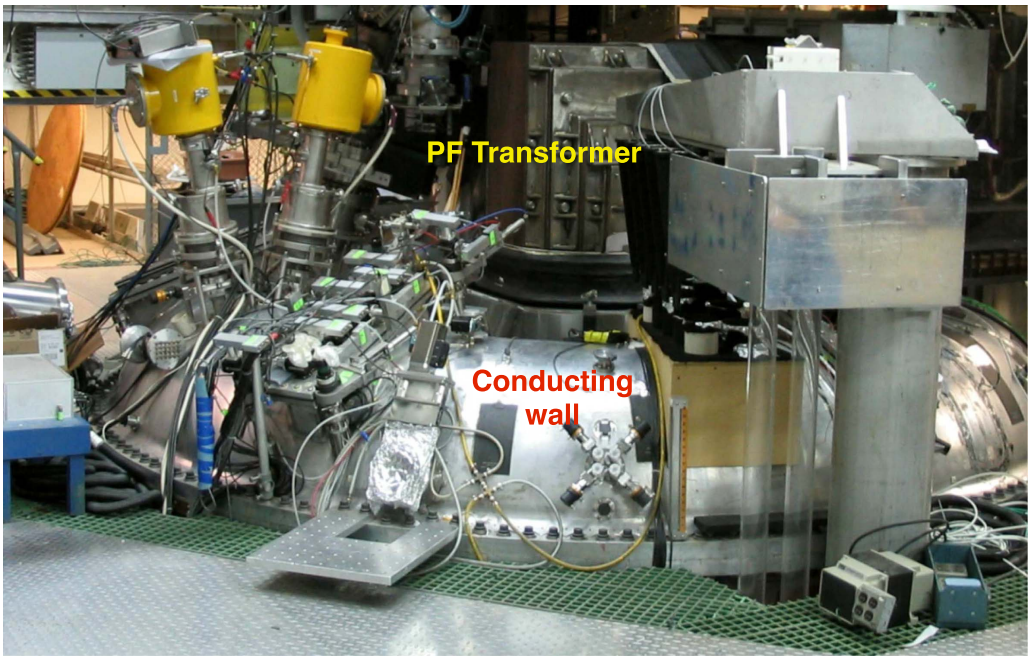

Figure 2. The MST experiment, showing the transformer and the conducting wall.

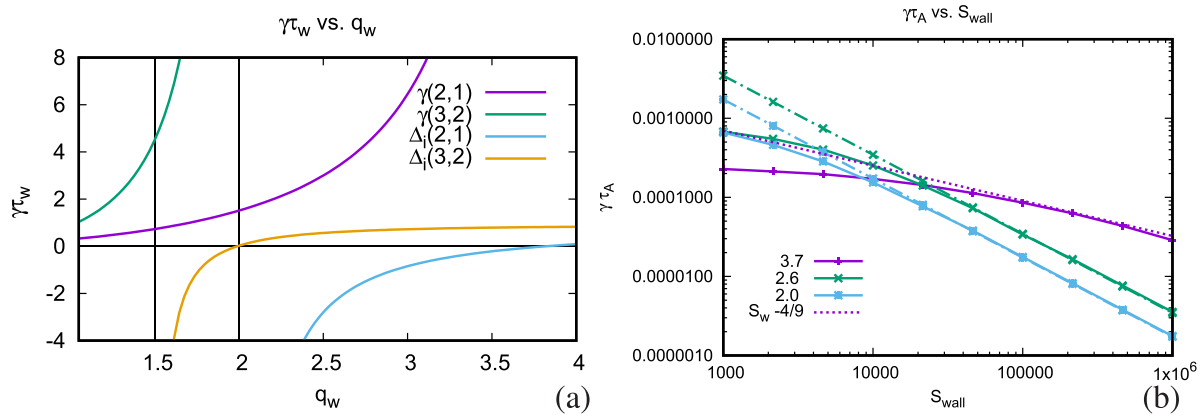

Figure 3. (a) Linear growth rate $\gamma\tau_{\rm wall}$ as a function of $q_{\rm w}$, for $(2,1)$ and $(3,2)$ modes. Also shown is Δ_i as a function of $q_{\rm w}$ for the two modes. When $\Delta_i < 0$ the mode is a RWTM or RWM. (b) Growth rate $\gamma\tau_{\rm A}$ as a function of $S_{\rm wall}$. The curves are labelled by the value of $q_{\rm w}$. The growth rate asymptotes to a RWM scaling for $S_{\rm wall} \gg S^{3/5}$, except for $q_{\rm w} = 3.7$ which asymptotes to $S_{\rm wall}^{-4/9}$.

In a step current model [15, 16] with a constant current density and $q = q_0$ contained within radius r_0, zero current density for $r > r_0$, $q = q_0(r/r_0)^2$, Then $q_{\rm w} = q_{\rm s}(r_{\rm w}/r_{\rm s})^2$, where q_0 is the value on axis and $q_{\rm s} = m/n$. In the model $q_a = q_{\rm w}$

$$\Delta_i = -2\frac{nq_0 - m + 1 - (r_0/r_{\rm w})^{2m}}{[nq_0 - m + 1 - (r_0/r_{\rm s})^{2m}][1 - (r_{\rm s}/r_{\rm w})^{2m}]}. \qquad (2)$$

It can be seen that as $r_{\rm s} \to r_{\rm w}$, that $\Delta_x, -\Delta_i \approx 2/[1 - (r_{\rm s}/r_{\rm w})^{2m}]$.

The growth rate is, neglecting the left side of (1),

$$\gamma\tau_{\rm wall} = -2m\frac{nq_0 - (m-1)}{nq_0 - (m-1) - (r_0/r_{\rm w})^{2m}}. \qquad (3)$$

This is also the growth rate of a RWM [15, 17] using the same model equilibrium. The crossover from RWTM to RWM occurs smoothly at $q_a = m/n$. For $q_a < m/n$, the mode becomes a RWM.

In figure 3(a) is plotted $\gamma\tau_{\rm wall}$ in (3) for the cases $q_0 = 1.08$, $(m,n) = (2,1)$, and $(3,2)$ as a function of $q_{\rm w}$. Also shown is Δ_i in (2). For $\Delta_i \geqslant 0$, the mode is a TM. For $(2,1)$, this occurs at $q_{\rm w} \geqslant 3.7$, in this model. There is a $(3,2)$ TM for $q_{\rm w} \geqslant 2.27$. For the $(2,1)$ mode, γ is in the regime of validity of (3) for $q_a \leqslant 1.98$. The $(3,2)$ is in this regime for $q_a \leqslant 1.7$. There is a pole in Δ_i when the denominator of (2) vanishes, at $r_{\rm s} = r_{\rm w}$ or $q_{\rm w} = m/n$. This is the transition from RWTM to RWM. At these values of $r_{\rm s}$ or $q_{\rm w}$, there is no pole in γ, so the transition from RWTM to RWM is smooth. There is a pole in γ at which the denominator of (3) vanishes.

This is the same as the zero of Δ_i, at which the RWTM becomes a TM.

The scaling of γ with $S_{\rm wall}$ is shown in figure 3(b). The curves were obtained by solving (1) with parameters $(m,n) = (2,1)$, $q_0 = 1.08$, $S = 10^5$, and several $q_{\rm w}$ values. For small $S_{\rm wall}$, the RWTM satisfies a no wall TM dispersion relation. For large $S_{\rm wall}$, except for the case $\Delta_i = 0$, with $q_{\rm w} = 3.7$, which has $\alpha = 4/9$, asymptotically γ is given by (3), plotted as dashed curves. The range of $S_{\rm wall}$ which deviates from (3) decreases as $q_{\rm w}$ decreases.

The model used here is consistent with simulations shown in the next sections. The RWTM and RWM have a growth time and TQ time proportional to $S_{\rm wall}$. The $(3,2)$ growth rate is larger than the $(2,1)$, while the simulations show that the nonlinear behavior is dominated by the $(2,1)$ mode for $q_a \geqslant 2$, and the $(3,2)$ for $q_a < 2$.

The TQ is caused by the growth of RWTMs and RWMs. The linear growth rates indicate the $S_{\rm wall}$ scaling of the TQ time, but are not sufficient to obtain $\tau_{\rm TQ}$ quantitatively. Nonlinear simulations are needed, which are described in the following.

3. Case $q_a = 2.6$

Nonlinear resistive MHD simulations are carried out with M3D [9] in which the resistive wall [10] time was varied. It is found that the MST is unstable to RWTMs and RWMs. The modes cause a TQ, on a timescale of order 200 ms, much longer than the experimental pulse of 50 ms.

The simulations used 16 poloidal planes, adequate to resolve low toroidal mode numbers. The simulations were dominated by $n = 1,2$ modes.

The simulations were initialized with equilibrium reconstructions in which q on axis $q_0 = 1$, and $q_a = 2.6, 2.0, 1.7$ and 1.5 at the edge. The initial profiles of q, RJ_ϕ, and T as a function of $x = R - R_0$, with $Z = 0$. are shown for the case $q = 2.6$ in figure 4.

Figure 5 shows contour plots from a simulation with $q_0, q_a = 1, 2.6$. It has $S_{\rm wall} = 3.3 \times 10^4$. The plots are at time $t = 5300\tau_{\rm A}$, near the end of the simulation. Figure 5(a) shows ψ, which appears distorted by a $(3,2)$ TM. The simulation contains $(3,2)$, and $(2,1)$ modes. Figure 5(b) shows the perturbed ψ, where $\tilde{\psi} = \psi - \psi_{\rm avg}$, and $\psi_{\rm avg}$ is the toroidal average. It predominantly has $(2,1)$ structure. Figure 5(c) is the temperature T.

Figure 6 shows the effect of wall penetration time $\tau_{\rm wall}$. Simulations were done with several values of $S_{\rm wall}$. Figure 6(a) shows the time history of the volume integrated pressure P. The value of $S_{\rm wall}$ is indicated by labels, with ∞ indicating an ideal wall. The TQ time is measured as the time difference $(t_{20} - t_{90})/0.7$, where t_{90} is the time at which the temperature is 90% of its peak, and t_{20} is the time when it has 20% of its peak value.

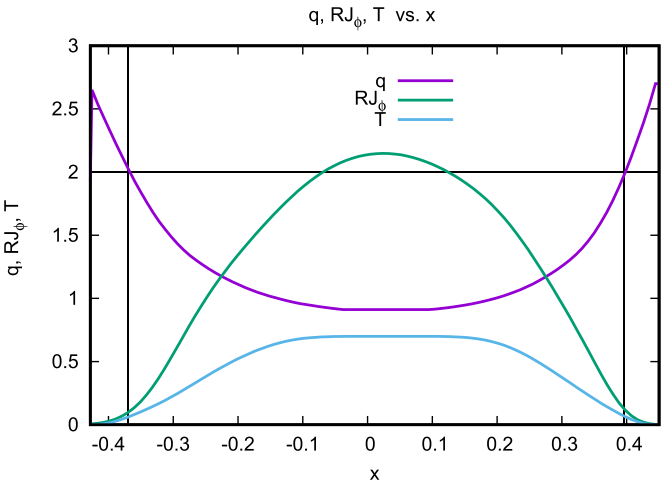

Figure 4. Initial profiles of q, RJ_ϕ, and T as a function of $x = R - R_0$, $Z = 0$. T is rescaled for visibility.

The values of $\tau_{\rm TQ}$ as a function of $S_{\rm wall}$ are collected in figure 6(b). They are fit with $0.22S_{\rm wall}$, and projected to the experimental value $S_{\rm wall} = 7 \times 10^5$, $\tau_{\rm TQ} \approx 1.5 \times 10^5 \tau_{\rm wall}$. This is $\tau_{\rm TQ} \approx 180$ ms, the data point for MST plotted in figure 1.

The magnetic perturbations consist of primarily a $(2,1)$, with a smaller amplitude $(3,2)$ mode. Figure 6(c) shows the magnetic energy in $n = 1,2$ toroidal harmonics of the normal component of magnetic field at the wall, given by $MW_n = \oint |\mathbf{B}(n) \cdot \hat{\mathbf{n}}/B|^2 {\rm d}l/L$, where $\mathbf{B}(n) = (2\pi)^{-1} \oint \mathbf{B} \exp(in\phi) {\rm d}\phi$, $L = \oint {\rm d}l$, $\hat{\mathbf{n}}$ is the unit normal to the wall, and l is the length along the wall for fixed toroidal angle ϕ. The time dependent increase in the rate of the pressure drop in figure 6(a) is caused by the growth of the amplitude of the magnetic perturbations.

4. Cases $q_a = 2, 1.7, 1.5$

It is possible to have $q_a \leqslant 2$ in MST [5]. The case $q_a = 2$ is at the borderline between RWTM and RWM. It has a much slower TQ than the case $q_a = 2.6$.

Figure 7(a) shows the TQ time as a function of $S_{\rm wall}$ for $q_a = 2$. Also plotted for comparison is $0.7S_{\rm wall}$. Projecting to the experimental $S_{\rm wall}$ gives $\tau_{\rm TQ} \approx 5 \times 10^5 \tau_{\rm A} \approx 0.57$ s. Figure 7(b) shows MW_n and P for $S_{\rm wall} = 10^4$. In this case the $(3,2)$ or $n = 2$ mode is dominant. The $(3,2)$ RWTM has a larger amplitude than the $(2,1)$ RWM.

Simulations were also performed for $q_a = 1.7$ and $q_a = 1.5$. The time history data is summarized in figure 8. Figure 8(a) shows $\tau_{\rm TQ}$ as a function of $S_{\rm wall}$ for $q_a = 1.7$. The data is fit by $\tau_{\rm TQ} \approx 0.4\tau_{\rm wall}$, which is projected to $\tau_{\rm TQ} \approx 1.15 \times 10^5 \tau_{\rm A}$, ≈ 0.13 s. Figure 8(b) shows $\tau_{\rm TQ}$ as a function of $S_{\rm wall}$ for $q_a = 1.5$. The data is fit by $\tau_{\rm TQ} \approx 0.13\tau_{\rm wall}$, which is projected to $\tau_{\rm TQ} \approx 0.9 \times 10^5 \tau_{\rm A}$, ≈ 0.10 s.

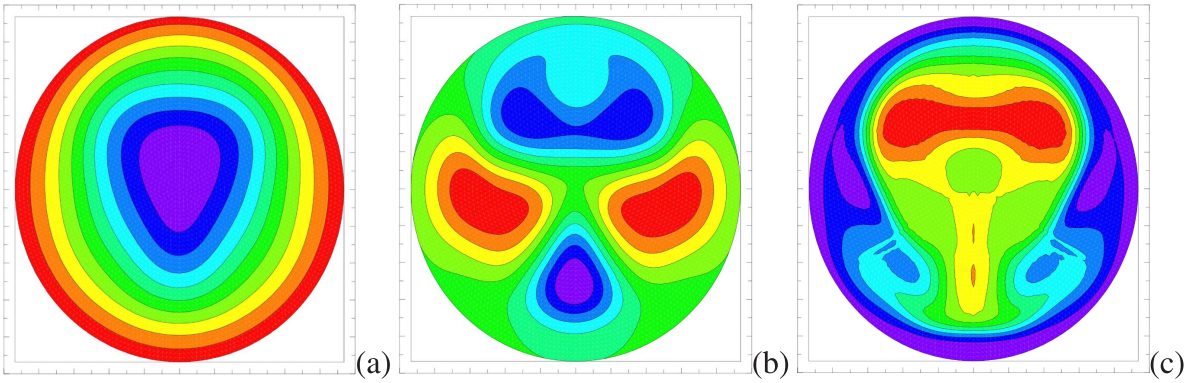

Figure 5. (a) Contour plot of ψ at time $t = 5300\tau_A$ for case with $q_a = 2.6$, $S_{\rm wall} = 3.3 \times 10^4$. (b) Contour plot of $\tilde{\psi}$ at the same time. (c) Temperature T at the same time.

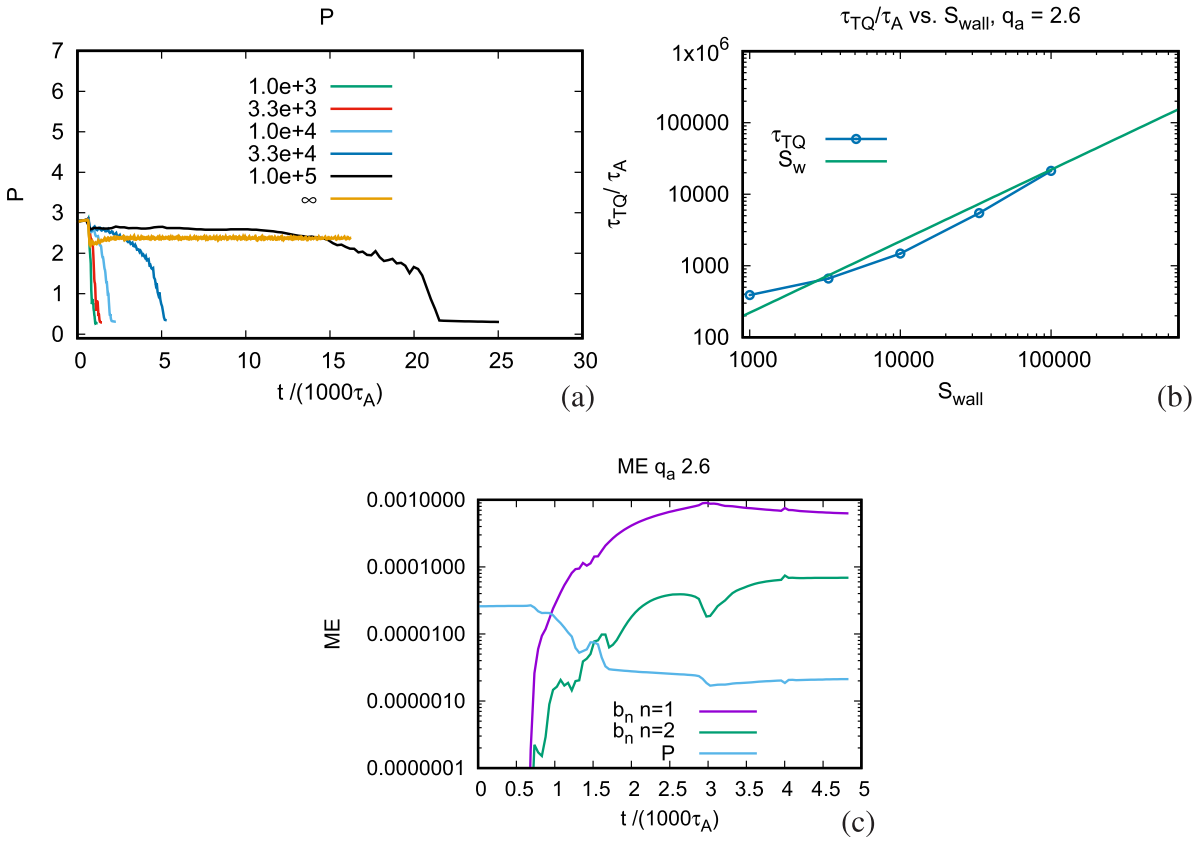

Figure 6. (a) Time history of total pressure P in simulations of MST with $q_a = 2.6$. The labels denote the value of $S_{\rm wall}$. The label ∞ is for an ideal wall. In that case there is no TQ. (b) TQ time $\tau_{\rm TQ}$ measured from the time histories. The projected TQ time at the experimental $S_{\rm wall} = 7 \times 10^5$ is $\tau_{\rm TQ} \approx 1.5 \times 10^5 \tau_A = 0.18\,$s. (c) Time history of MW_n, the energy of $n = 1,2$ components of normal magnetic field at the wall, dominated by a $(2,1)$ mode, and P, for $S_{\rm wall} = 10^4$.

The TQ time data is summarized in figure 9, showing $\tau_{\rm TQ}$ as a function of q_a, at the experimental value of $S_{\rm wall}$. Except for $q_a = 2$, the values of $100\,{\rm ms} < \tau_{TQ} < 200\,{\rm ms}$. The $q_a = 2$ case is much slower, $\tau_{\rm TQ} = 570\,$ms. Also shown in figure 9 is $1/\gamma$ where $\gamma\tau_{\rm wall}$ is taken from figure 3(a), using $\gamma(2,1)$ for $q_a \geqslant 2$, and $\gamma(3,2)$ for $q_a < 2$. The slow TQ at $q_{\rm w} = 2$ is also seen in the model linear growth times. The agreement of simulations and theory is remarkable, considering the simplicity of the model used to obtain (3).

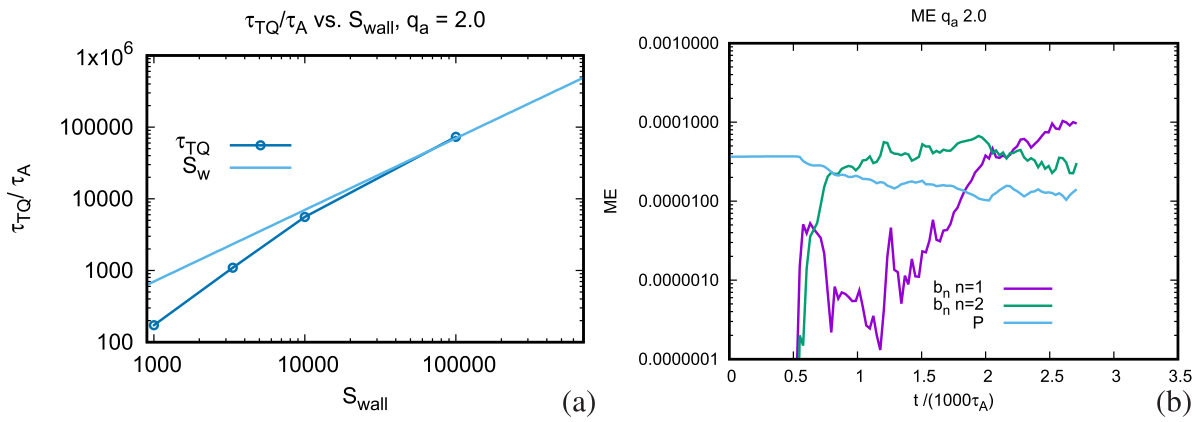

Figure 7. (a) Plots of τ_{TQ}/τ_A, and $0.7S_{wall}$. The projected TQ time at the experimental S_{wall} is $\tau_{TQ} \approx 5 \times 10^5 \tau_A = 0.57$ s. (b) Time history of MW_n, wall magnetic normal magnetic energies, and P, for $S_{wall} = 10^4$.

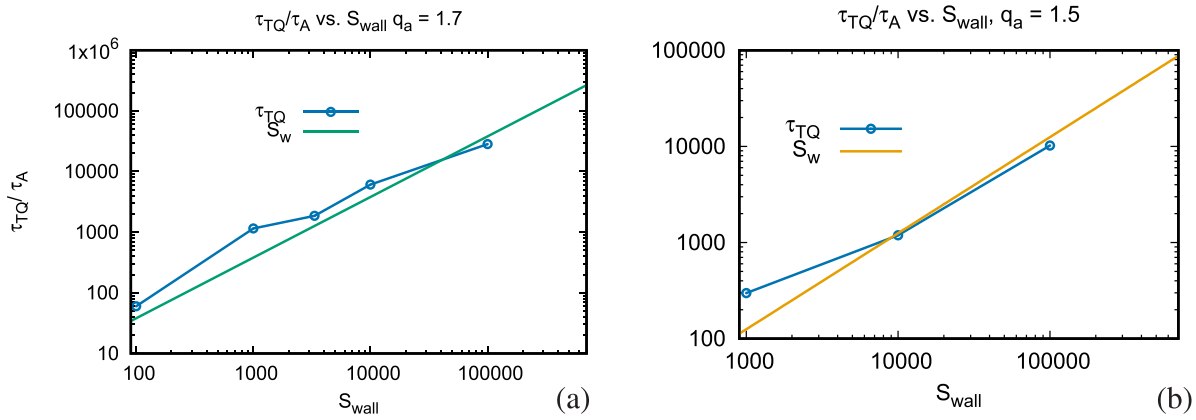

Figure 8. (a) TQ time τ_{TQ} measured from the time histories, for $q_a = 1.7$. The fit is $\tau_{TQ} \approx 0.4\tau_{wall}$, which is projected to $\tau_{TQ} \approx 1.15 \times 10^5 \tau_A$, ≈ 0.13 s. (b) τ_{TQ} as a function of S_{wall}, for $q_a = 1.5$. Here $\tau_{wall} \approx 0.13\tau_{wall}$, which is projected to $\tau_{TQ} \approx 0.9 \times 10^5 \tau_A$, ≈ 0.10 s.

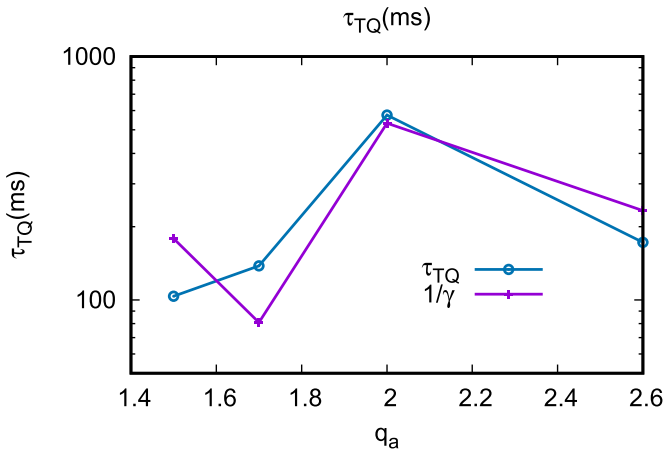

Figure 9. τ_{TQ} as a function of q_a, from the simulations, and $1/\gamma$ from figure 3(a).

5. Conclusions

MST was originally operated as a RFP, which required a highly conducting, close fitting wall. When run as a tokamak, the MST does not have major disruptions. This is consistent with simulations with $S_{wall}^{-1} = 0$, which is an ideal wall. When the wall is made resistive in the simulations, RWTMs become unstable and cause a TQ. The TQ time increases linearly

with $\tau_{\rm wall}$. This is characteristic of large $\tau_{\rm wall}$, $S_{\rm wall} \gg S^{3/5}$. Asymptotically the RWTM satisfies the RWM dispersion relation, except when $\Delta_i \approx 0$. MST has large $S_{\rm wall}$, as does ITER when $S \ll 10^9$ in the edge.

Nonlinear simulations examined four cases, with edge $1.5 \leqslant q_a \leqslant 2.6$. In all cases, the TQ time $\tau_{\rm TQ} \geq 100$ ms, compared to the experimental pulse time 50 ms. This is shown in figure 9.

The TQ time from the $q_a = 2.6$ case was plotted in figure 1, since this case more nearly resembles a standard tokamak. The implication for other tokamaks is that a more conducting wall slows the RWTM and mitigates disruptions, especially in ITER.

Data availability statement

All data that support the findings of this study are included within the article (and any supplementary files).

Acknowledgments

We thank Jay Anderson for help with the MSTFit code. This work was supported by U.S. DOE under Grants DE-SC0020127, DE-SC0020245, and DE-SC0018266.

ORCID iDs

H R Strauss https://orcid.org/0000-0002-2740-1889
N C Hurst https://orcid.org/0000-0003-3016-5239

References

[1] Strauss H (JET Contributors) 2021 Effect of resistive wall on thermal quench in JET disruptions *Phys. Plasmas* **28** 032501
[2] Strauss H 2021 Thermal quench in ITER disruptions *Phys. Plasmas* **28** 072507
[3] Strauss H, Lyons B C and Knolker M 2022 Locked mode disruptions in DIII-D and application to ITER *Phys. Plasmas* **29** 112508
[4] Dexter N, Kerst D W, Lovell T W, Prager S C and Sprott J C 1991 The Madison Symmetric Torus *Fusion Technol.* **19** 131
[5] Hurst N C *et al* 2022 Self-organized magnetic equilibria in tokamak plasmas with very low edge safety factor *Phys. Plasmas* **29** 080704
[6] Marrelli L , Martin P, Piuatti M E, Sarff J S, Chapman B E, Drake J R, Escande D F and Masamune S 2021 The reversed field pinch *Nucl. Fusion* **61** 023001
[7] Gribov Y and Pustovitov V D 2002 Analytical study of RWM feedback stabilisation with application to ITER *Proc. 19th IAEA Fusion Energy Conf. (Lyon, 2002) CT/P-12* (available at: http://www-pub.iaea.org/MTCD/publications/PDF/csp_019c/pdf/ctp_12.pdf)
[8] Hanson J M *et al* 2014 Feedback-assisted extension of the tokamak operating space to low safety factor *Phys. Plasmas* **21** 072107
[9] Park W, Belova E, Fu G Y, Tang X, Strauss H R and Sugiyama L E 1999 Plasma simulation studies using multilevel physics models *Phys. Plasmas* **6** 1796
[10] Pletzer A and Strauss H 2011 *Comput. Phys. Commun.* **182** 2077
[11] Anderson J K, Forest C B, Biewer T M, Sarff J S and Wright J C 2004 *Nucl. Fusion* **44** 162
[12] Gimblett C G 1986 On free boundary instabilities induced by a resistive wall *Nucl. Fusion* **26** 617
[13] Bondeson A and Persson M 1988 Stabilization by resistive walls and q-limit disruptions in tokamaks *Nucl. Fusion* **28** 1887
[14] Betti R 1998 Beta limits for the N = 1 mode in rotating - toroidal - resistive plasmas surrounded by a resistive wall *Phys. Plasmas* **5** 3615
[15] Finn J A 1995 Resistive wall stabilization of kink and tearing modes *Phys. Plasmas* **2** 198
[16] Furth H P, Rutherford P H and Selberg H 1973 Tearing mode in the cylindrical tokamak *Phys. Fluids* **16** 1054
[17] Liu Y, Albanese R, Portone A, Rubinacci G and Villone F 2008 An analytical demonstration of coupling schemes between magnetohydrodynamic codes and eddy current codes *Phys. Plasmas* **15** 072516